Neurochemical Research (2022) 47:3355–3368
https://doi.org/10.1007/s11064-022-03688-9

ORIGINAL PAPER

Identification of ADP/ATP Translocase 1 as a Novel Glycoprotein and Its Association with Parkinson's Disease

Wenli Zhang[1] · Jun Liu[2] · Qianhui Chen[1] · Wenyong Ding[1] · Sheng Li[1] · Li Ma[2]

Received: 3 April 2022 / Revised: 10 July 2022 / Accepted: 12 July 2022 / Published online: 13 August 2022

Abstract

Protein glycosylation plays a crucial role in central nervous system, and abnormal glycosylation has major implications for human diseases. This study aims to evaluate an etiological implication of the variation in glycosylation for Parkinson's disease (PD), a neurodegenerative disorder. Based on a PD mouse model constructed by the intraperitoneal injection with 1-Methyl-4-phenyl-1,2,3,6-tetrahydropyridine, glycosylation variation was accessed using biotinylated lectin of dolichos biflorus agglutinin (DBA) specific for the exposed N-acetylgalactosamine linked to glycoprotein. Consequently, a glycoprotein with a significantly reduced N-acetylgalactosamination was identified as ADP/ATP translocase 1 (ANT1) by lectin affinity chromatography coupled with MALDI-TOF MS/MS (mass spectrometry), and confirmed by the analysis of dual co-immunofluorescence and Western blot. A tissue-specific distribution of de-N-acetylgalactosaminated ANT1 was found to be correlated with high risk of PD. At cellular level, an obvious co-aggregation between ANT1 and DBA was only found in the MPP^+-induced PD-like cell model using dual co-immunofluorescence. Thus, we found that ANT1 was a potential glycoprotein with terminal N-acetylgalactosamine moiety, and the variation of glycosylation in ANT1 was associated with PD. This investigation provides an innovative insight in protein glycosylation with PD pathogenesis.

Keywords ADP · ATP translocase 1 · Parkinson's disease · N-acetylgalactosamine · Glycosylation · ANT1 · DBA

Introduction

Parkinson's disease (PD), a chronic and progressive neurodegenerative disorder, is the second most common neurodegenerative disease after Alzheimer's disease [1, 2]. A conservative estimate of worldwide prevalence of PD is 0.3%, but rises sharply to > 3% in the population at more than the eighth decade of life. Compared with the general population, the increase in the disease mortality is not evident in the first decade after the disease onset, but goes up by twice with disease progression thereafter. Especially, current improvement in health care leads to a longer survival, which is related to an increasing prevalence of the disease over time and causes a widespread concern in the study of Parkinson disease. Therefore, a progressive increase in the societal, personal and economic burden associated with PD is expected in the future as the world population ages [3].

Pathologically, PD is the result of selective degeneration of dopaminergic neurons in the *substantia nigra pars compacta* (*SNpc*), and distinctive Lewy body inclusions that are composed mainly of α-synuclein in the brain and peripheral nerves [4]. The dopaminergic neurons are involved in transmitting dopamine from *SNpc* to another basal ganglia nucleus and striatum. Degeneration of these neurons results in the deterioration of motor activities, the major manifestations of PD. Lewy bodies are insoluble fibrillary aggregates that damage nerve cells, and α-synuclein is believed to play a pathological role in the progression of PD [4, 5].

Although remarkable achievements in the understanding of PD pathogenesis have been made during the over 200-year history of research, the ultimate underlying cause of PD still remain scanty currently [6]. Moreover, the diagnostic criteria of parkinsonism are still based on the identification of motor symptoms, whereas the onset of the disease

✉ Sheng Li
lisheng_1996@163.com

✉ Li Ma
mali_lele@sina.com

[1] Biochemistry and Molecular Biology Department of College of Basic Medical Sciences, Dalian Medical University, Dalian, China

[2] Department of Epidemiology, Dalian Medical University, Dalian, China

precedes the first symptoms of classic motor disturbances by decades [2, 4]. Even the new diagnostic criteria are applied now, the misdiagnosis rate is still high. Therefore, there is a strong need to understand the molecular mechanism on the pathogenesis and etiology of PD, further to identify and discover reliable biomarkers for PD. The aim of the present study was to exploit neurodegenerative disease-associated proteins with disturbed glycosylation patterns, thereby accelerating our understanding of the molecular basis on an oligosaccharide variation in PD pathogenesis.

Proteins accounted for one fifth of all proteins in databases are heavily glycosylated in eukaryotes. Protein glycosylation, the enzymatic addition of N-linked or O-linked oligosaccharide moieties to glycoproteins, is one of the most common posttranslational modifications of many functional proteins, and has a profound effect on numerous biological processes including cell–cell interactions, cell signal transduction, subcellular and extracellular trafficking, etc. The oligosaccharide moieties of glycoprotein also affect protein structures via contributing to protein conformation, stability, folding, and solubility [7–10]. Glycosylation plays particularly crucial roles in central nervous system (CNS) too [10]. For example, DAT (dopamine transporter), an N-glycosylated protein, has been demonstrated that the N-glycosylated DAT transports DA more efficiently than its non-glycosylated form which is related to PD [7]. Abnormal glycosylation has major implications for human health. However, it remains unclear whether defective protein glycosylation plays a role in the pathogenesis of PD.

In this study, we aimed at elucidating an association of defective glycosylation with the neuropathology of PD, further to investigate the molecular mechanism of PD etiology and pathogenesis. Toward this purpose, the lectin of dolichos biflorus agglutinin (DBA) which traps glycopeptides with α-linked N-acetylgalactosamine was used to examine the glycosylation status in the different specialized brain structures in mouse model that can faithfully recapitulate the pathological aspects of PD.

Materials and Methods

Construction of the MPTP-Treated PD Mouse Model

C57BL/6 male mice (20–25 g and 8 to 10-week-old) was used to construct the mouse model by the intraperitoneal injection with 1-Methyl-4-phenyl-1,2,3,6-tetrahydropyridine (MPTP) as described previously [11]. Sixth of mice was randomly and evenly divided into two groups: control (n = 30) and MPTP (n = 30). The injection was performed unilaterally with MPTP (2.925 μg/μL in physiological saline, 10 μl/g) for 10 times at intervals of 3.5 days in the MPTP group. The mice received the same volume of physiological saline (10 μL/g) via intraperitoneal injection were used as a control in this study.

Cell Culture and Cell Treatment

Neuroblastoma SH-SY5Y cells were routinely grown in Dulbecco's modified Eagle's medium (DMEM) supplemented with 10% (v/v) heat-inactivated fetal bovine serum (FBS), 2 mmol/L L-glutamine and 100 units/mL of penicillin-streptomycin. Cells were grown at 37 °C in a humidified incubator containing 5% carbon dioxide. When the cells reached 70% confluence, 1.2 mmol/L MPP^+ was added into the medium to induce PD-like neurotoxicity.

Cell Viability Assay

Cell viability was measured by MTT (3-[4,5-dimethylthiazol-2-yl]-2,5-diphenyltetrazolium bromide) assay in this study. The exponentially growing SH-SY5Y cells were seeded in a 96-well plate at a density of 1×10^4 cells/well. When the cells reached 70% confluence, the medium was replaced with fresh medium with or without 1.2 mmol/L MPP^+ in the absence of FBS. cells were then incubated for the subsequent 24 h. The MPP^+-treated or untreated cells were incubated with 100 μL of MTT solution (0.5 mg/mL in PBS) at 37 °C for another 4 h. Cell supernatant was then removed by centrifugation, and 200 μL of DMSO was added to each well to dissolve formazan crystals. Optical density was detected with a microplate reader (Thermo Scientific) at 490 nm. Each experiment was performed independently in triplicate.

Preparation of Protein Lysates

The mice were sacrificed by cervical dislocation, then the isolated brains of mice were rinsed with ice-cold 0.9% physiological saline. The following steps were all performed on ice. The different specialized structures of mouse brains, including striatum, midbrain, cerebellum, cortex, hippocampus, brain stem, were dissected carefully. The samples for each structure were then placed in a small homogenizer, and homogenized in ice cold RIPA lysis buffer [50 mmol/L Tris (pH7.4) containing 150 mmol/L NaCl, 1% Triton X-100, 1% sodium deoxycholate, 0.1% SDS and 1 mmol/L PMSF]. The insoluble fragments in homogenate were removed by centrifugation at 14,000 rpm for 30 min twice. The SH-SY5Y cells cultured in a 10 cm dish were digested with trypsin follow by collection with centrifugation at 1000 rpm for 5 min. The collected SH-SY5Y cells were then broken by ultrasonication (5 S on, 3 S off), and the cell lysate was cleared by centrifugation at 14,000 rpm for 30 min twice. A protein determination was then performed using a BCA kit

(keyGEN BioTECH, China). The prepared protein lysates were frozen at − 80 °C for a further investigation.

Processing of Fixed Brain Tissues

The fixation of whole mouse brains was processed as described previously [12]. The mice were anesthetized by inhalation of diethyl ether, and then intracardially perfused with 0.9% physiological saline and 4% paraformaldehyde in phosphate-buffered saline (PBS; 50 mmol/L of NaH_2PO_4; 5 mmol/L of KCl; 1.5 mmol/L of $MgCl_2$; and 80.1 mmol/L of NaCl; pH 7.4) for 30 min respectively through the opened heart. The whole mouse brains were quickly removed and fixed in 4% paraformaldehyde, then saturated in 15% picric acid in PBS followed by storage in 20% sucrose in PBS at 4 °C for a further immunofluorescence staining.

Western Blot Analysis (WB)

Eighty microgram of total proteins for each different specialized structure was denatured and resolved on a 12% SDS-acrylamide gel electrophoresis (SDS-PAGE) gel. Proteins separated on the gel were transferred onto polyvinylidene difluoride (PVDF) membrane in blotting buffer (20 mmol/L Tris-base, 150 mmol/L glycine and 20% methanol). For immunodetection, the PVDF membrane was blocked with 5% skim milk dissolved in TBST (20 mmol/L Tris-HCl, 0.1% Tween 20, 137 mmol/L NaCl, and pH 7.6) for 2 h at room temperature, and incubated with a primary antibody at 4 °C overnight. The primary antibodies for Western blot analysis contained biotinylated DBA (Vector Laboratories), monoclonal antibodies including anti-β-actin antibody (Abcam), anti-tyrosine hydrolase (TH) antibody (Abcam) and anti-ADP/ATP translocase 1 antibody (anti-ANT1, Abcam) in this study. The membranes were then washed three times with TBST and incubated with horseradish peroxidase-linked avidin or secondary antibodies for 40 min. After the membranes were rinsed with TTBS, they were treated with an enhanced chemiluminescence (ECL system) according to the manufacturer's instructions (GE Healthcare Bio-Sciences Corp.).

Immunofluorescence Staining of the Mouse Brains

The whole mouse brain saturated in 20% sucrose in phosphate-buffered saline (PBS) was frozen in Milli-Q water in freezing microtome/cryostat (-40 °C), and cut into around six micron-thick sections which were mounted on glass slides for immunofluorescence analyses. Tissue sections were treated with avidin for inactivating endogenous biotin and incubated with 3% bovine serum albumin (BSA) for preventing the nonspecific binding. Then, the sections were treated with a primary antibody including anti-ADP/ATP translocase 1 monoclonal antibody and biotinylated DBA. Subsequently, the sections were incubated with streptavidin-FITC and secondary antibodies conjugated to rhodamine, and counterstained with 4′,6-diamidino-2-phenylindole (DAPI). The fluorescent images were captured with a fluorescence microscope.

Immunofluorescence Assays of the Cells

Neuroblastoma SH-SY5Y cells were seeded on sterile coverslips and grown at a confluency of 70%. The cells were then fixed in 4% formaldehyde in PBS at 25 °C for 15 min and permeabilized using 0.5% v/v Triton X-100 at 25 °C for 10 min after three-time wash using PBS. Following several washes in PBS to remove any residual detergents, a 5% BSA solution in PBS (w/v) was added onto the coverslips to block the non-specific binding of the primary and secondary antibodies, and kept at 37 °C for 1 h. The cells on the coverslips were incubated with primary antibodies or biotinylated DBA at 4 °C for overnight after washing in PBS. The coverslips were then washed three times using PBS and incubated with FITC/rhodopsin-conjugated avidin/secondary antibodies in PBS containing 1% BSA at 37 °C for 1 h. The cell nuclei were visualized by DAPI counterstaining. The coverslips were then imaged using a fluorescence microscope.

Lectin Affinity Purification

The pre-equilibrated GSLII (Griffonia simplicifolia lectin II) agarose (Vector Laboratories)/DBA agarose of 1.0 mL column volume was equilibrated with 5 mL equilibration buffer (20 mmol/L Tris-HCl, pH 8.0, 0.15 mol/L NaCl, 1 mmol/L $MnCl_2$ and 1 mmol/L $CaCl_2$). The cytoplasmic fraction of mouse brain was applied to the column. The column was then washed with 10 mL washing buffer (20 mmol/L Tris-HCl, pH 8.0, 0.15 mol/L NaCl, 1 mmol/L $MnCl_2$, 1 mmol/L $CaCl_2$ and 40 mmol/L N-acetyl-galactosamine) followed by elution with 5 mL elute buffer (20 mmol/L Tris-HCl, pH 8.0, 0.15 mol/L NaCl, 1 mmol/L $MnCl_2$, 1 mmol/L $CaCl_2$ and 200 mmol/L N-acetyl-galactosamine). And 500 µL elute for each tube was collected for identifying glycoproteins which specifically interacted with GSLII via galactose or N-acetyl-galactosamine of sugar chains. Final protein concentration of eluted fractions was determined using a BCA kit. The eluted fractions were analyzed by running a 12% SDS-PAGE, and the visualization of protein bands was performed using a silver staining kit (Sigma, St. Louis, MO, USA).

MS/MS Analysis

Protein identification in gel was performed using Mass spectrometry in this study. The target protein band in a silver-stained gel was excised into small pieces, and decolorized in

100 mmol/L NH_4HCO_3/30% ACN containing 100 mmol/L $Na_2S_2O_3$: 300 mm $K_3Fe(CN)_6$ (1:1). The decolorized gel was then digested by 12.5 ng/μL trypsin with sequencing-grade in 100 mmol/L NH_4HCO_3 solution at 37 °C for 20 h according to a modified in-gel trypsin digestion procedure. Next, the trypsin-digested peptide fragments were desalted using C18 StageTip column and lyophilized. The lyophilized peptide fragments were dissolved in 0.1% formic acid for subsequent tandem mass spectrometry (MS/MS) analysis.

MS/MS experiments were performed using a 5800 MALDI-TOF/TOF MS (Applied Biosystems), and conducted in positive ionization mode and automatic data acquisition mode. The optimal source/gas parameters were set as follows: the instrument contained a Nd:YAG laser; the mass analyzer scan was 800–4000 Da *m/z*; the ions were accelerated with a voltage of 2 kV; the list of peptides of interest meant for the fragmentation analyses was manually defined in the equipment's current settings with 2 kV collision energy and CID off. The MS data retrieval was performed using Mascot 2.2 software against NCBI database.

Image Quantification and Statistical Analyses

The protein bands in the images of Western blot were quantified using the Image J software with subtracting background density, and the immunofluorescence signals in the immunofluorescence staining graphs were processed using Image-Pro Plus software (version 6.0). The density of protein bands and immunofluorescence signals were analyzed and plotted using PRISM 6 software.

The statistical analysis between the MPTP-treated mice and the control mice was performed using a two-tailed equal variance Student's *t*-test. Results are presented as mean ± SEM. Significance was set at a *P* values less than 0.05. Each experiment was independently repeated at least three times.

Results

Mice with Parkinsonian Symptoms Were Successfully Established

In this study, a widely acceptable PD animal model was established by administrating MPTP. To evaluate whether the mice intraperitoneally injected with MPTP displayed the same typical symptoms as PD patients, the impairment of motor function was observed and the representative biological indexes related to PD were analyzed. Consequently, the motor dysfunctions, including a significant increase in latency of vertical grid test which is to assess the forepaw strength, and a dramatic reduction in latency of horizontal grid test which is to evaluate the forepaw faults, were found in the MPTP-treated mice. In addition, the alteration in the representative parkinsonian indexes related to PD, including a reduction of DA and 5-HT in striatum, and a decrease of TH in *SNpc*, were revealed in the MPTP-treated mice compared to the control mice. Thus, a successful PD mouse model was established as depicted previously [12].

A Glycoprotein with a Significantly Reduced N-acetylgalactosamination in the MPTP-Treated Mice was Identified as ANT1

To evaluate the changes of the exposed N-acetylgalactosamine linked to glycoproteins, a 12% SDS-PAGE separation followed by Western blot analysis blotted with biotinylated DBA was conducted in this study. The optical density ratio of glycoprotein to β-actin was statistically analyzed using Image J. Figure 1A shows that Western blot analysis identifies more than one band that interacts specifically with DBA, and reveals a changeable density of glycoproteins in the brains of PD mice. As determined by Western blot analysis using biotinylated DBA, an target glycoprotein at the molecular weight of 35–40 (indicated by the arrow in Fig. 1A) displayed a significant reduction in N-acetylgalactosamination in the MPTP-treated mice compared to the control mice (Fig. 1D).

To identify the target glycoprotein, an affinity chromatography analysis coupled with mass spectrometry was conducted in this study. An agarose-conjugated GSLII, which specifically traps galactose and N-acetylgalactosamine, was utilized for purifying glycoproteins from the homogenate of brain tissues. The purified glycoproteins were analyzed by 12% SDS-PAGE followed by silver-staining as shown in Fig. 1B. The band with similar molecular weight on the silver-stained gel to the target glycoprotein detected by immunoblotting against DBA was chosen for MS identification (as shown by the arrow in Fig. 1B).

The silver-stained gel containing the target protein was digested using trypsin followed by investigation for deciphering its primary structure by tandem mass spectrometric analysis (MS/MS). The MALDI-TOF MS data and mass spectrums were shown in Fig. 2. The MALDI-TOF MS data that met the criteria of protein score ≥ 50 at 95% confidence level (protein score C.I. %) in the dataset allowed the identification of the target glycoprotein. In this study, the MS analysis resulted in identification of ADP/ATP translocase 1 (ANT1) as shown in Fig. 2A.

The mass spectra of the target glycoprotein as shown in Fig. 2B resulted in 11 molecular fragment ions after collision induced dissociation. Of 11, the predominant ions at *m/z* 856.5, 902.4, 1004.5, 1044.4, 1169.6, and 1507.8 indicated the presence of GNLANVIR, GAWSNVLR, QIFLGGVDR, RMMMQSGR, EQGFLSFWR, and IPKEQGFLSFWR, respectively. In addition, the detected fragment ions *m/z*

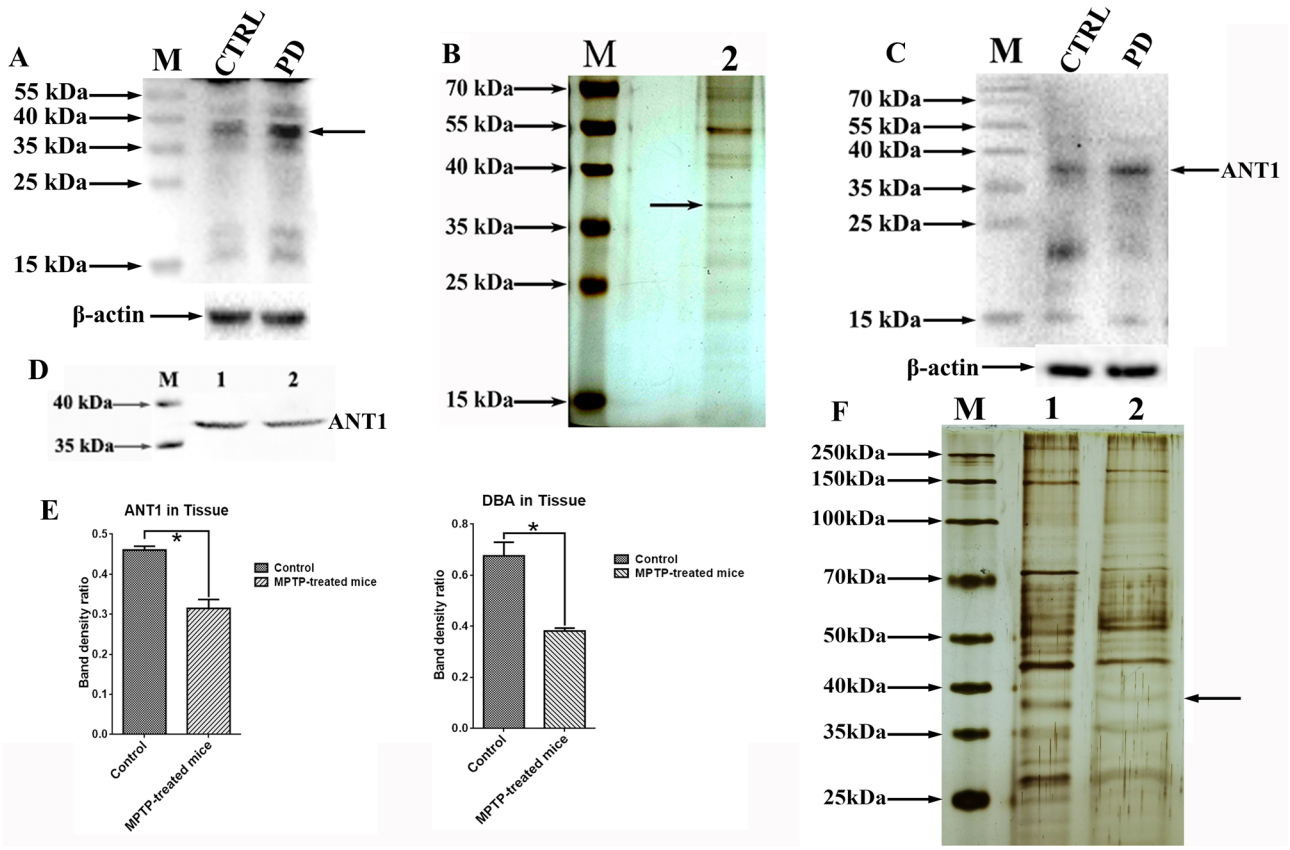

Fig. 1 Recognition, purification and confirmation of ANT1 as a glycoprotein containing α-linked N-acetylgalactosamine. PD, MPTP-treated mice; CTRL, control. 1, total protein of mouse brains; 2, glycoproteins purified by lectin-agarose affinity chromatography. **A** Western blot analysis on glycoproteins with α-linked N-acetylgalactosamine. The bands were visualized using an ECL kit. The target glycoprotein was shown by the arrow. M, PageRuler prestained protein ladder (Fermentas). **B** SDS-PAGE analysis of the purified glycoproteins. The gel was stained using silver staining. The target glycoprotein was shown by the arrow. **C** Western blot analysis on ANT1 protein. The membrane was probed with the monoclonal anti-ANT1 antibody, the bands were visualized using the ECL kit. M, PageRuler prestained protein ladder (Fermentas). **D** Western blot analysis on the glycoproteins purified by agarose bound-DBA. The membrane was probed with the monoclonal anti-ANT1 antibody, the bands were visualized using the ECL kit. M, Multicolor Prestained Protein ladder (WJ 103, 10–250 kDa, Yamei, China). **E** Densitometric analysis of the target glycoprotein with α-linked N-acetylgalactosamine (DBA in Tissue) and soluble ANT1 (ANT1 in Tissue) normalized to β-actin. The statistical analyses were performed by a two-tailed equal variance Student's *t*-test; Bars represented the mean ± SEM; *, $P < 0.05$. **F** SDS-PAGE analysis of the glycoproteins purified by agarose bound-DBA. The gel was visualized by silver staining. M, Multicolor Prestained Protein ladder (WJ 103, 10–250 kDa, Yamei, China)

1219.6, 1253.6, 1446.6, 2326.1, and 2796.3 corresponded to DFLAGGIAAAVSK, EFNGLGDCLTK, YFPTQALNFAFK, MGDQALSFLKDFLAGGIAAAVSK, and YFAGNLASGGA AGATSLCFVYPLDFAR, respectively. Sequence alignment demonstrated that all of the above identified fragment ions were generated by the trypsin-digested ANT1. Additionally, the tandem mass spectrometry (MS/MS) spectrum of m/z 1169.56 showed the prevalent b ions including *m/z* 112, 315.13, 416.19, 462.18, 644.29, 738.32 and y ions including *m/z* 175.12, 344.18, 578.25, 1040.56 (Fig. 2C). Among those ions, *m/z* 175.12 corresponding to arginine, *m/z* 1040.56 corresponding to QGFLSSFWR were detected as predominant ions, and *m/z* 112 was generated from glutamate residue (129) ions by a loss of water. The spectrum also showed ions *m/z* 344.18, 578.25, 644.29 originated by a neutral loss of NH_3 from the fragmentation of WR, SFWR, EQGFLS, respectively. These data confirmed that the *m/z* 1169.56 was composed of EQGFLSSFWR which only appeared in the trypsin-digested ANT1 according to sequence alignment analysis.

Thus, based on MALDI-TOF spectral analysis, the structural elucidation indicates that the target glycoprotein is ANT1.

Confirmationof ANT1 as a Glycoprotein Using Dual Immunolabeling of ANT1/DBA and WesternBlot Analysis Against Anti-ANT1 Antibody Coupled with Lectin Affinity Isolation

To confirm that the identified ANT1 was a glycoprotein, a Western bolt analysis using the monoclonal anti-ANT1

A

Protein Name	Accession No. (NCBI)	Protein MW (D)	Protein PI	Pep. Count	Protein Score	Protein Score C. I. %
ADP/ATP translocase 1	gi|21903382	32883.1	9.73	11	72	98.08

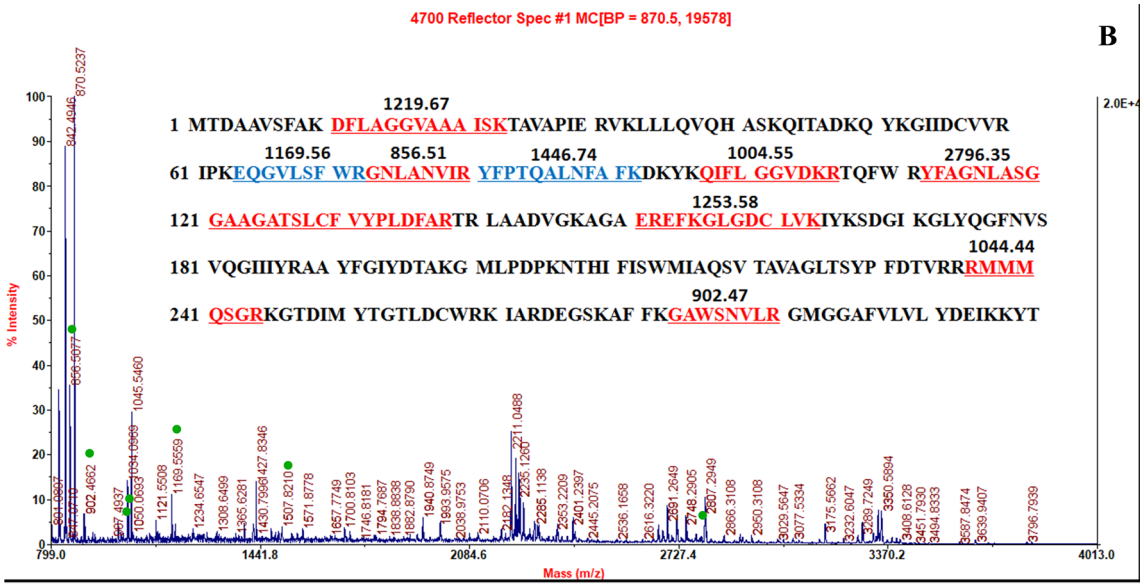

Fig. 2 Identification of ANT1 as a glycoprotein via the lectin affinity chromatography coupled with MALDI-TOF MS/MS. **A** Profiles of identified ANT1 in Mus musculus. **B** MALDI-TOF MS spectrum of the identified ANT1. The green dots showed the identified trypsin-digested ANT1 peptide fragment ions; the inset figure displayed the identified trypsin-digested ANT1 peptide fragments in red or blue. **C** Tandem MS spectrum of the trypsin-digested ANT1 peptide fragment ions with m/z 1169.56: EQGFLSFWR. The inset spectrograms showed the tandem MS spectrum of trypsin-digested ANT1 peptide fragment with an m/z 1169.56

antibody as a probe was performed. Figure 1C shows a clear band at molecular weight ranging from 35 to 40 kDa on the membrane, and its size was similar to the target band detected by immunoblotting with DBA. Therefore, Western blot analysis demonstrated that the monoclonal anti-ANT1 antibody was highly suspected to interact with the same protein as the one recognized by DBA.

To further confirm that ANT1 was glycosylated, in situ dual co-immunofluorescence analysis was performed in mouse brain. Figure 3 shows a clear expression of glycoproteins (DBA) and ANT1 (ANT1) in mouse brain. Figure 3 demonstrates the co-localization of ANT1 with glycoproteins using merged images (DBA + ANT1 and DBA + ANT1 + DAPI). Consequently, the co-localization analysis indicated that ANT1 was co-localized with glycoprotein containing α-linked N-acetylgalactosamine oligosaccharides. Thus, the co-expression of ANT1 within glycoproteins confirmed that ANT1 was a glycoprotein containing an α-linked N-acetylgalactosamine oligosaccharides.

In addition, to further verify whether ANT1 was glycosylated, an affinity chromatography was used to isolate total glycoproteins from mouse brains using agarose bound-DBA as a medium, followed by Western blot analysis using monoclonal anti-ANT1 antibody as the probe. Although there were multiple bands in the silver-stained gel as shown in Fig. 1F, D confirms that ANT1 is in the purified mixture of glycoproteins. Thereby, this data strongly supported that ANT1 was a glycoprotein with an α-linked N-acetylgalactosamine oligosaccharides.

Combining the mass spectral data with in-situ dual co-immunofluorescence staining and Western blot analysis on the glycoproteins purified by DBA-agarose affinity chromatography, the target glycoprotein with an α-linked N-acetylgalactosamine is suggested to be ANT1.

Low Level of N-acetylgalactosaminated ANT1 was Associated with PD

To characterize the relationship between N-acetylgalactosaminated ANT1 and PD, we analyzed the abundance of N-acetylgalactosaminated ANT1 in the different specialized structures of the mouse brains including hippocampus, cortex, striatum, cerebellum, midbrain and brain stem. Figure 4A shows that the N-acetylgalactosaminated ANT1 is expressed at variable levels in the different brain structures. To examine the association of the N-acetylgalactosaminated ANT1 with PD, the relative abundance of N-acetylgalactosaminated ANT1 was assessed using Image J as shown in Fig. 4B.

Contrast analyses revealed that a significant reduction in N-acetylgalactosaminated ANT1 was found in cortex (CTRL: 0.273 ± 0.035; PD: 0.180 ± 0.030; $P = 0.025$), midbrain (CTRL: 0.338 ± 0.056; PD: 0.183 ± 0.032; $P = 0.014$), striatum (CTRL: 0.469 ± 0.069; PD: 0.136 ± 0.047; $P = 0.002$), hippocampus (CTRL: 0.197 ± 0.023; PD: 0.083 ± 0.014; $P = 0.002$), and brain stem (CTRL: 0.500 ± 0.108; PD: 0.111 ± 0.025; $P = 0.004$) in the MPTP-treated mice, with the exception of cerebellum. A dramatical increase in N-acetylgalactosaminated ANT1 was found in cerebellum (CTRL: 0.185 ± 0.040; PD: 0.271 ± 0.027; $P = 0.036$) in the MPTP-treated mice. Despite of the reverse trend of ANT1 N-acetylgalactosamination in cerebellum, we found that the ANT1 was under-acetylgalatosaminated in the MPTP-treated mice compared to the control mice. This suggests that the low level of N-acetylgalactosaminated ANT1 is correlated with PD.

Reduced N-acetylgalactosaminated ANT1 was Associated with High Risk of PD

To exclude the possibility of the reduced ANT1 N-acetylgalactosamination resulted from the decreased ANT1 protein in expression as illustrated previously [12], and further to investigate whether the N-acetylgalactosaminated ANT1 was associated with PD, a co-expression analysis on ANT1 and glycoproteins with N-acetylgalactosamine oligosaccharides was performed using double-immunofluorescence analysis. The monoclonal anti-ANT1 antibody specifically recognizes ANT1 in red, and biotinylated DBA specifically interacts with N-acetylgalactosamine oligosaccharides linked to glycoprotein in green. The co-localization of ANT1 with glycoproteins was analyzed using the merged images. Figure 5A demonstrates an apparent expression and distribution of glycoproteins and ANT1 in the mouse brains. The co-localization analysis indicated that ANT1 was partially N-acetylgalactosaminated as shown in Fig. 5. Figure 5B also shows a significant reduction in the ratio of the N-acetylgalactosaminated ANT1 to total ANT1 occurred in the different structures of the mouse brains including hippocampus ($P = 0.018$; − 81.8%), cortex ($P = 0.044$; − 68.6%), striatum ($P = 0.022$; − 57.1%), midbrain ($P = 0.001$; − 88.4%) and brain stem ($P = 0.019$; − 68.3%) in the MPTP-treated mice compared to the control mice, with the exception of cerebellum. There was no significant difference detected in cerebellum ($P = 0.647$) between the MPTP-treated mice and their controls. That results were consistent with the ones from Western blot analysis. So, it was suggested that ANT1 was under-N-acetylgalactosaminated under PD conditions. Thus, in situ dual co-immunofluorescence analysis indicates that the under-N-acetylgalactosaminated ANT1 is associated with a high risk of PD.

Aggregation of Glycosylated ANT1 was Found in Neuroblastoma SH-SY5Y Cells Treated with MPP^+

PD-like cell model was constructed by adding MPP^+ in the neuroblastoma SH-SY5Y cells in this study. SH-SY5Y cells

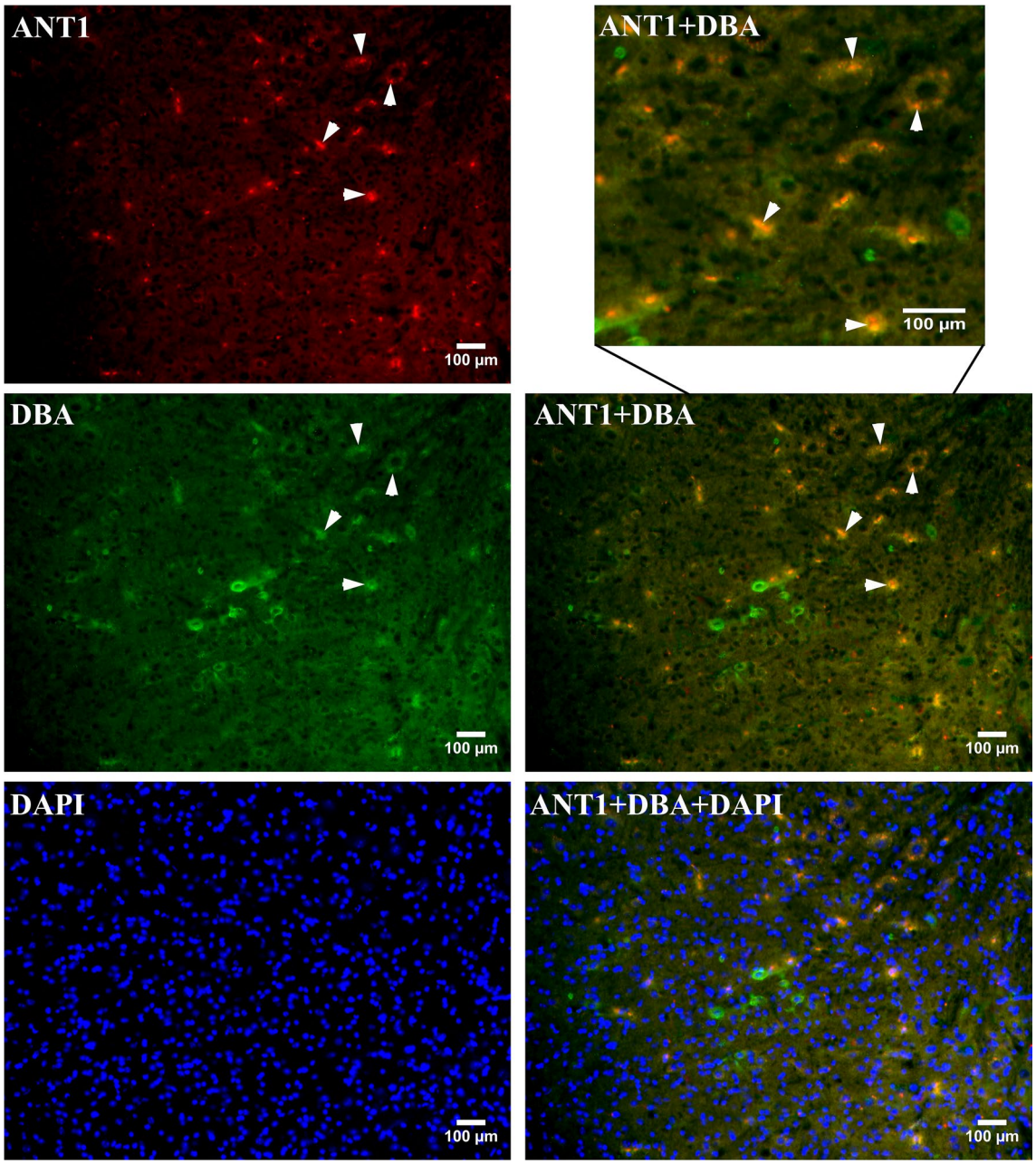

Fig. 3 Confirmation of ANT1 as a glycoprotein via dual immunofluorescence analysis. The micrographs were taken in brain stem of mouse brain at magnification of 200. Red signals corresponded to ANT1 stained by anti-ANT1 monoclonal antibody (ANT1). Green signals corresponded to the glycoproteins detected by DBA (DBA). Blue signals corresponded to DAPI-stained nuclei (DAPI). Co-localization of ANT1 with DBA was shown as the merged images of green and red (ANT1 + DBA), a dual immunolabeling of ANT1/DBA was visible in orange, and a double expression of ANT1 with glycoprotein was indicated by white tips. Co-localization of ANT1 with DBA was shown as the merged images of green, red and blue (ANT1 + DBA + DAPI)

were treated with MPP^+ in concentrations ranging 0.5–4.5 mmol/L for 24 h, then cell survival was evaluated by MTT assay. The curve of cell viability against MPP^+ concentration was plotted as shown in Fig. 6A. The plot revealed a significant reduction in cell viability in a concentration-dependent manner. Especially, MPP^+ at concentrations of 2 mmol/L killed more than 50% of cells. Consequently, 1.2 mmol/L MPP^+ was determined to induce neuroblastoma SH-SY5Y cells to generate parkinsonism symptoms. Apart from cell viability assay to verify the neurotoxicity treated by MPP^+, the representative parkinsonian parameters, including DA and TH, were analyzed in this study. DA was examined using HPLC as shown in Fig. 6B, D. Contrast analyses on HPLC data revealed that cytosolic DA was dramatically decreased

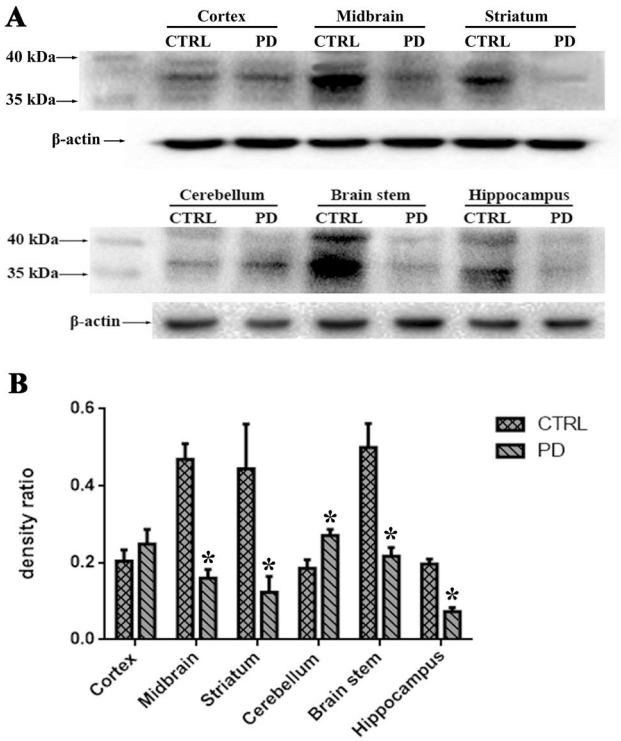

Fig. 4 Tissue-specific expression of N-acetylgalactosaminated ANT1 in various structures of the mouse brains. Cell lysates containing 80 μg soluble proteins were subjected to Western blot analysis coupled with 12% SDS-PAGE separation. CTRL, control; PD, the MPTP-treated PD mice. **A** Western blot analysis on N-acetylgalactosaminated ANT1. The membrane was probed with biotynilated DBA and visualized using an ECL kit. M, PageRuler prestained protein ladder (Fermentas). **B** Densitometric analysis of N-acetylgalactosaminated ANT1 normalized to the level of β-actin. The analyses were conducted by a two-tailed equal variance Student's *t*-test. Bars represented the mean ± SEM; *, $P < 0.05$

in the MPP^+-treated cells compared to the untreated cells. TH abundance was evaluated by Western blot analysis as illustrated in Fig. 6C, D. A significant reduction in TH abundance was found in the MPP^+-treated cells relative to their controls. Thus, the reduction in TH abundance and DA content demonstrated that the MPP^+-treated cells generated a representative PD-like variation.

Based on the cell model induced by MPP^+, the level of N-acetylgalactosaminated ANT1 was detected using Western blot assay as depicted in Fig. 6E. Statistical analysis on band density showed that glycosylated ANT1 was significantly reduced in the MPP^+-treated cells compared to the untreated cells (Fig. 6D), which was consistent with the evidences at the animal level. To further confirm the N-acetylgalactosamination of ANT1, in situ dual co-immunofluorescence analysis was conducted at cellular level. The fluorescent signals with brightly red or green were considered as positive, otherwise negative. Figure 6F shows a clear deposition of ANT1 in the MPP^+-treated cells. Unregular and enlarged color spots in red, which represented ANT1 deposition, were only found in the MPP^+-treated cells compared to the untreated cells which displayed an evenly dispersed distribution with small size. In addition, the co-localization of ANT1 with glycoproteins using merged images revealed that ANT1 was co-localized with glycoproteins containing α-linked N-acetylgalactosamine moieties, and the co-expressed fluorescence signals in the form of aggregated bunches were only found in the MPP^+-treated cells compared to the untreated cells as shown in Fig. 6F. Additionally, the enlarged micrograph in Fig. 6F indicated that the aggregated bunches located in cytosol. Thereby, the co-expression analysis of ANT1 within glycoproteins suggested that ANT1 with an α-linked N-acetylgalactosamine oligosaccharides was highly suspected to have an important implication for PD pathogenesis, and it promoted the protein aggregation upon MPP^+-induced neurotoxicity.

Discussion

In this study, the glycosylation of ADP/ATP translocase 1 (ANT1) was found to be associated with PD. ANT1, also known as the adenine nucleotide translocator 1, adenine nucleotide translocase 1, or ADP/ATP carrier 1, is the most abundant protein in the inner membrane of mitochondria, constituting up to 10% of total mitochondrial proteins [13]. ANT1 participates in the exchange of cytosolic adenosine diphosphate (ADP) and mitochondrial adenosine triphosphate (ATP) across the inner mitochondrial membrane, and is the main mitochondrial ADP/ATP exchanger with major metabolic implications [14]. Apart from a major role of ANT1 as an adenosine nucleotide transporter, ANT1 is involved in formation of pro-apoptotic mPTP (mitochondrial permeability transition pore) and mediates FA-dependent uncoupling of proton efflux [15, 16].

Nowadays, ANT1 have been intensively studied in myocardial contractile system [17–20] and tumor [21–23]. However, little is known about ANT1 contributing to PD, with the exception of our recent study which illustrates that the down-regulated ANT1 is related to PD via forming a protein aggregate with α-synuclein [12]. In this study, ANT1 is firstly identified as a glycoprotein with the N-acetylgalactosamine oligosaccharides. Actually, the posttranslational modification of ANT1 has been reported previously. Currently, several independent studies have focused on the importance of the posttranslational modification in ANT1. For example, nitroalkylation of Cys_{57} in ANT1 has been reported to have an implication in distinct physiological role of ANT1. This irreversible modification of Cys_{57} is involved in stimulating mild mitochondrial uncoupling, reducing ADP/ATP transport via ANT, and preventing mPTP opening in the post-ischemic state [13, 24]. In addition, the

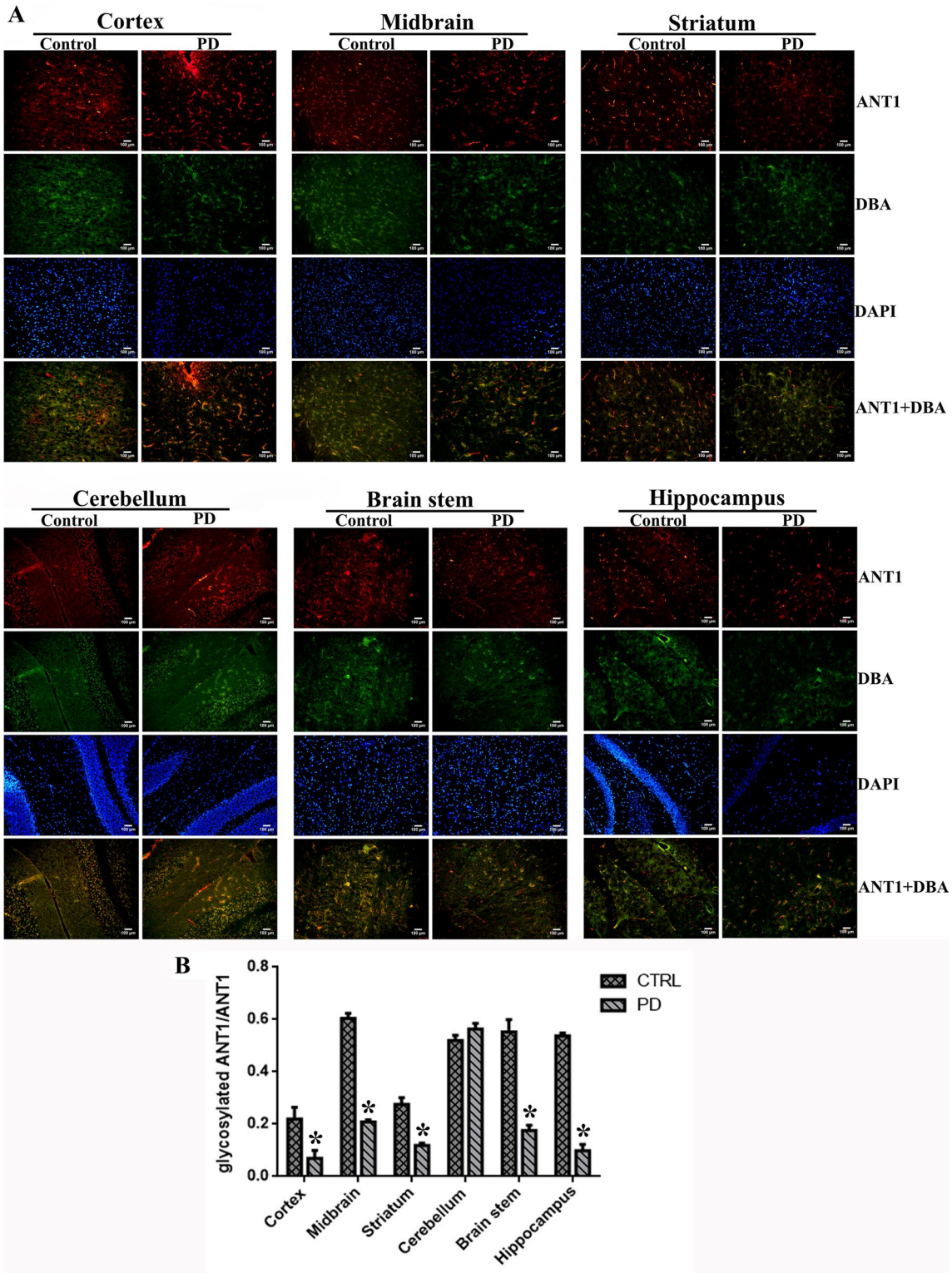
A
Cortex
Control
PD
Midbrain
Control
PD
Striatum
Control
PD
ANT1
DBA
DAPI
ANT1+DBA
Cerebellum
Control
PD
Brain stem
Control
PD
Hippocampus
Control
PD
ANT1
DBA
DAPI
ANT1+DBA
B
glycosylated ANT1/ANT1
0.0
0.2
0.4
0.6
0.8
CTRL
PD
Cortex
Midbrain
Striatum
Cerebellum
Brain stem
Hippocampus

◂**Fig. 5** Dual immunofluorescence analysis on the glycoproteins with N-acetylgalactosamine oligosacchrides and ANT1 in the different specialized structures of mouse brains. **A** Representative micrographs of dual immunofluorescence analysis taken at magnification of 200. Green signals corresponded to the glycoproteins detected by DBA; Red signals corresponded to ANT1 stained by anti-ANT1 monoclonal antibody; Blue signals corresponded to DAPI-stained nuclei; Co-localization of ANT1 with DBA was shown as the merged images of green and red; Co-localization of ANT1 with DBA was shown as the merged images of green and red. **B** Statistical analysis of the immunofluorescence signals between the MPTP-treated mice and the control mice. Glycosylated ANT1/ANT1 represented the ratio of the N-acetylgalactosaminated ANT1 to total ANT1. The analyses were conducted by a two-tailed equal variance Student's *t*-test. Bars represented the mean ± SEM; *, $P < 0.05$

mammalian ANT isoforms including ANT1, ANT2, and ANT3 were documented to be methylated at Lys-52 [13]. Presently, the methylation of ANTs at Lys-52 have been identified to be catalyzed by the methylase of FAM173A. Additionally, Lys-52 was pointed out to be exclusively trimethylated, demonstrating that the methylation at Lys-52 is constitutive, rather than regulatory and dynamic [25]. The posttranslational modification of ANT1 has a profound implication in bioenergetic effects and mPTP formation. However, the report on the glycosylation of ANT1 remains scanty now. Our study illustrated that the form of ANT1 de-N-acetylgalactosamination is associated with PD. Based on the evidences obtained in this study, it was suggested that de-N-acetylgalactosaminated ANT1 may be a defective factor to cause PD.

In addition, our study showed a tissue-specific distribution of glycosylated ANT1. A significant decrease was found in striatum, midbrain, hippocampus and brainstem. Theoretically, there are four major dopaminergic pathways in brains, which are the nigrostriatal pathway/mesostriatal pathway, mesocortical pathway, mesolimbic pathway and tuberoinfundibular pathway. Among these, the nigrostriatal pathway initiates from SNpc in midbrain and ends in striatum, and it particularly plays an important role in regulating cognition, motor behavior, and sleep-wake states [26, 27]. Nigrostriatal pathway is the efferent connection of DA between the SNpc where DA synthesizes and striatum. A marked reduction in dopamine function in nigrostriatal pathway is most pronounced pathological features of PD. Therefore, Parkinson's disease is characterized by degeneration of the nigrostriatal dopaminergic system, resulting in the motor features of the disease [28]. Based on our study, a dramatic decrease in ANT1 glycosylation in nigrostriatal dopaminergic system was revealed. Therefore, it is conceivable that a reduction in the levels of the nigrostriatal ANT1 glycosylation could be involved in brain disorders and contributes to the pathophysiology of PD.

Although our data showed that ANT1 was a glycoprotein, but the composition and structure of sugar chains linked to ANT1 remained undiscovered. So, based on ANT1 sequence in homo sapient, a prediction on its glycosylation was performed. The sequence of ANT1 was retrieved from the public online database: https://www.ncbi.nlm.nih.gov/protein/NP_001142.2. Nuclear-encoded ANT1 was 298-amino-acid polypeptide with a mass of 33.064 kDa and an isoelectric point of 9.78. ANT1 was predicted to be a transmembrane-associated polypeptide with 3 transmembrane regions at 112–134, 172–194 and 209–231. A critical region of ANT1 at 102–141 had been identified to be required for apoptosis [23]. In addition, ANT1 was highly conserved in mammalian species. The homology in the coding sequences of ANT1 extended remarkable to 96% between homo sapient and rattus norvegicus, and to 95% between homo sapient and mus musculus. For the glycosylation prediction of ANT1, six highly potential O-linked glycosylation sites were predicted at the region of Ser_6, Thr_{154}, Thr_{196}, Ser_{212}, Thr_{251} and Thr_{253} respectively by MOE (Molecular Operating Environment) software package. Certainly, the glycosylation sites of ANT1 are needed to be further identified by experimental evidences. Additionally, the compositional and structural identification of ANT1 oligosaccharide moiety, and the relationship between ANT1 glycosylation and pathogenesis of PD are required to be determined in a further study as well.

Conclusions

As noted, we reported that the under-N-acetylgalactosaminated ANT1 and suspicious glycosylated ANT1 accumulation were associated with PD pathogenesis. Despite the limitations of this study, this is the first report to demonstrate ANT1 as a glycoprotein with N-acetygalatosamine oligosaccharides, and to reveal de-N-acetylgalactosaminated ANT1 as a potential etiology of PD. This investigation provides key information necessary for designing prospective studies to evaluate N-acetylgalactosaminated ANT1 in the etiology of PD, thus potentially promotes an innovative understanding of the protein glycosylation on the etiology of PD and provides valuable information on developing potential drug targets in PD treatment or reliable biomarkers in PD prognostication.

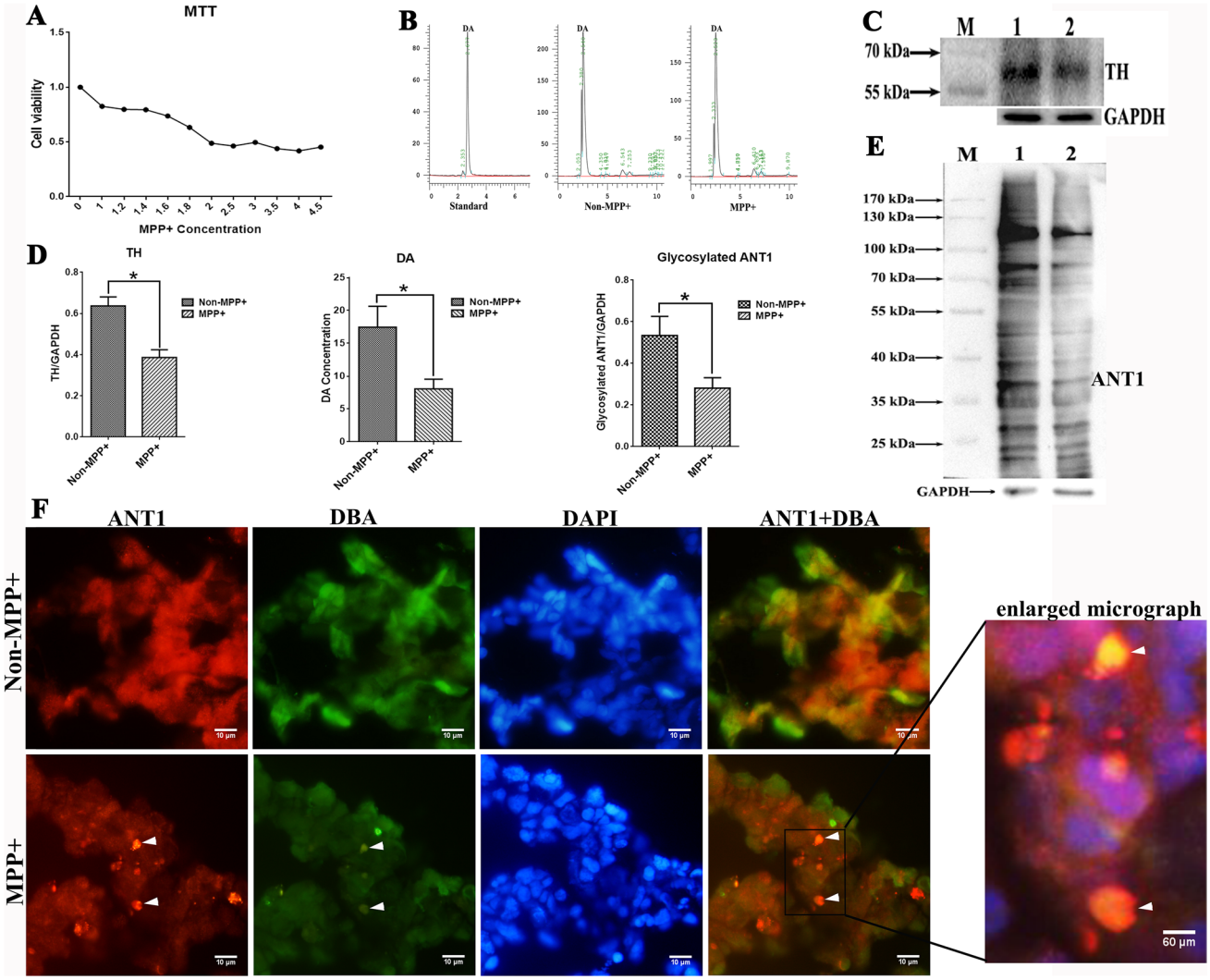

Fig. 6 Co-aggregation analysis of ANT1 with glycoproteins containing N-acetylgalactosamine oligosaccharides at cellular level. 1 or non-MPP$^+$, untreated SH-SY5Y cells; 2 or MPP$^+$, MPP$^+$-treated SH-SY5Y cells. M, PageRuler prestained protein ladder (Fermentas). **A** Effects of MPP$^+$ on the viability of SH-SY5Y cells. Cell viability was assessed by MTT assay and plotted by cell viability against MPP$^+$ concentration ranging from 0 to 4.5 mmol/L. **B** Representative HPLC images on cytosolic DA and its standard. **C** Analysis on intracellular TH abundance in SH-SY5Y cells using Western blot analysis. Cells lysates containing 60 μg soluble proteins were subjected to Western blot analysis coupled with 12% SDS-PAGE separation. The membrane was probed with monoclonal anti-TH antibody and visualized using an ECL kit. **D** Statistical analysis on intracellular levels of DA, TH and glycosylated ANT1 between the MPP$^+$-treated and untreated SH-SY5Y cells. The statistical analyses were conducted by a two-tailed equal variance Student's *t*-test; bars represented the mean ± SEM; *, $P < 0.05$. **E** Expression analysis on glycosylated ANT1 in SH-SY5Y cells. Eighty microgram of total protein was applied. The membrane was probed with DBA, and the visualization of bands was performed using an ECL kit. **F** Dual immunofluorescence analysis on the co-aggregation of ANT1 with glycoproteins containing N-acetylgalactosamine moieties in SH-SY5Y cells. Visualization was performed using a fluorescence microscopy at magnification of 400. Red signal corresponded to ANT1; Green signal corresponded to glycoproteins containing N-acetylgalactosamine moieties; Blue signal corresponded to DAPI-stained nuclei; Co-expression of ANT1 with glycoproteins containing N-acetylgalactosamine moieties was shown as the merged images of green and red. The co-aggregation regions were indicated by white tips. The enlarged micrograph was the amplification of the boxed area which resulted from the merged images of green, red and blue

Supplementary Information The online version contains supplementary material available at https://doi.org/10.1007/s11064-022-03688-9.

Funding This work was supported in part by National Natural Science Foundation of China (81200989, 81272429), Natural Science Foundation of Liaoning (2019-MS-088), Innovation Team Foundation of Liaoning (LT2010026), and Liaoning Provincial Program for Top Discipline of Basic Medical Sciences.

Data availability Data will be made available on reasonable request.

Declarations

Conflict of interest The authors declare that they have no conflicts of interest with this article.

Ethicalapproval of the study protocol This study was carried out in accordance with the principles of the Basel Declaration and recommendations of Dalian Medical University for laboratory animals. The protocol was approved by the Animal Ethics Committee of Dalian Medical University.

References

1. Li T, Le W (2020) Biomarkers for Parkinson's disease: how good are they? Neurosci Bull 36:183–194
2. Pajares M, Manda AIR, Bosca G, Cuadrado L (2020) A inflammation in Parkinson's disease: mechanisms and therapeutic implications. Cells 9:1687
3. Poewe W, Seppi K, Tanner CM, Halliday GM, Brundin P, Volkmann J, Schrag AE, Lang AE (2017) Parkinson disease. Nat Rev Dis Primers 3:17013
4. Liddle RA (2018) Parkinson's disease from the gut. Brain Res 1693:201–206
5. Lotankar S, Prabhavalkar KS, Bhatt LK (2017) Biomarkers for Parkinson's disease: recent advancement. Neurosci Bull 33:585–597
6. Grayson M (2016) Parkinson's disease. Nature 538(7626):S1
7. Afonso-Oramas D, Cruz-Muros I, Alvarez de la Rosa D, Abreu P, Giraldez T, Castro-Hernandez J, Salas-Hernandez J, Lanciego JL, Rodriguez M, Gonzalez-Hernandez T (2009) Dopamine transporter glycosylation correlates with the vulnerability of midbrain dopaminergic cells in Parkinson's disease. Neurobiol Dis 36:494–508
8. Frappaolo A, Sechi S, Kumagai T, Karimpour-Ghahnavieh A, Tiemeyer M, Giansanti MG (2018) Modeling congenital disorders of N-linked glycoprotein glycosylation in *Drosophila melanogaster*. Front Genet 9:436
9. Vicente Miranda H, Szego EM, Oliveira LMA, Breda C, Darendelioglu E, de Oliveira RM, Ferreira DG, Gomes MA, Rott R, Oliveira M, Munari F, Enguita FJ, Simoes T, Rodrigues EF, Heinrich M, Martins IC, Zamolo I, Riess O, Cordeiro C, Ponces-Freire A, Lashuel HA, Santos NC, Lopes LV, Xiang W, Jovin TM, Penque D, Engelender S, Zweckstetter M, Klucken J, Giorgini F, Quintas A, Outeiro TF (2017) Glycation potentiates alpha-synuclein-associated neurodegeneration in synucleinopathies. Brain 140:1399–1419
10. Koles K, Lim JM, Aoki K, Porterfield M, Tiemeyer M, Wells L, Panin V (2007) Identification of N-glycosylated proteins from the central nervous system of *Drosophila melanogaster*. Glycobiology 17:1388–1403
11. Ma L, Song J, Sun X, Ding W, Fan K, Qi M, Xu Y, Zhang W (2019) Role of microtubule-associated protein 6 glycosylated with Gal-(β-1,3)-GalNAc in Parkinson's disease. Aging 11(13):4597–4610
12. Ding W, Qi M, Ma L, Xu X, Chen Y, Zhang W (2021) ADP/ATP translocase 1 protects against an alpha-synuclein-associated neuronal cell damage in Parkinson's disease model. Cell Biosci 11:130
13. Nadtochiy SM, Zhu QM, Urciuoli W, Rafikov R, Black SM, Brookes PS (2012) Nitroalkenes confer acute cardioprotection via adenine nucleotide translocase 1. J Biol Chem 287:3573–3580
14. Hoshino A, Wang WJ, Wada S, McDermott-Roe C, Evans CS, Gosis B, Morley MP, Rathi KS, Li J, Li K, Yang S, McManus MJ, Bowman C, Potluri P, Levin M, Damrauer S, Wallace DC, Holzbaur ELF, Arany Z (2019) The ADP/ATP translocase drives mitophagy independent of nucleotide exchange. Nature 575:375–379
15. Bertholet AM, Chouchani ET, Kazak L, Angelin A, Fedorenko A, Long JZ, Vidoni S, Garrity R, Cho J, Terada N, Wallace DC, Spiegelman BM, Kirichok Y (2019) H transport is an integral function of the mitochondrial ADP/ATP carrier. Nature 571:515–520
16. Divakaruni AS, Brand MD (2011) The regulation and physiology of mitochondrial proton leak. Physiology (Bethesda Md) 26:192–205
17. Baines CP, Molkentin JD (2009) Adenine nucleotide translocase-1 induces cardiomyocyte death through upregulation of the pro-apoptotic protein Bax. J Mol Cell Cardiol 46:969–977
18. Narula N, Zaragoza MV, Sengupta PP, Li P, Haider N, Verjans J, Waymire K, Vannan M, Wallace DC (2011) Adenine nucleotide translocase 1 deficiency results in dilated cardiomyopathy with defects in myocardial mechanics, histopathological alterations, and activation of apoptosis. JACC Cardiovasc Imaging 4:1–10
19. Wang Y, Ebermann L, Sterner-Kock A, Wika S, Schultheiss HP, Dorner A, Walther T (2009) Myocardial overexpression of adenine nucleotide translocase 1 ameliorates diabetic cardiomyopathy in mice. Exp Physiol 94:220–227
20. Winter J, Hammer E, Heger J, Schultheiss HP, Rauch U, Landmesser U, Dörner A (2019) Adenine nucleotide translocase 1 expression is coupled to the HSP27-mediated TLR4 signaling in cardiomyocytes. Cells 8:1588
21. Jang J-Y, Choi Y, Jeon Y-K, Aung KCa, Kim C-W, (2008) Overexpression of adenine nucleotide translocase 1 (ANT1) induces apoptosis and tumor regression in vivo. BMC Cancer 8:1–9
22. Bauer MK, Schubert A, Rocks O, Grimm S (1999) Adenine nucleotide translocase-1, a component of the permeability transition pore, can dominantly induce apoptosis. J Cell Biol 147(7):1493–1502
23. Zamora M, Meroño C, Viñas O, Mampel T (2004) Recruitment of NF-κB into mitochondria is involved in adenine nucleotide translocase 1 (ANT1)-induced apoptosis. J Biol Chem 279:38415–38423
24. Nadtochiy SM, Baker PR, Freeman BA, Brookes PS (2009) Mitochondrial nitroalkene formation and mild uncoupling in ischaemic preconditioning: implications for cardioprotection. Cardiovasc Res 82:333–340
25. Małecki JM, Willemen H, Pinto R, Ho AYY, Moen A, Eijkelkamp N, Falnes P (2019) Human FAM173A is a mitochondrial lysine-specific methyltransferase that targets adenine nucleotide translocase and affects mitochondrial respiration. J Biol Chem 294:11654–11664
26. Raczka KA, Mechias ML, Gartmann N, Reif A, Deckert J, Pessiglione M, Kalisch R (2011) Empirical support for an involvement of the mesostriatal dopamine system in human fear extinction. Transl Psychiatry 1:e12–e12

27. Huang D, Xu J, Wang J, Tong J, Bai X, Li H, Wang Z, Huang Y, Wu Y, Yu M, Huang F (2017) Dynamic changes in the nigrostriatal pathway in the MPTP mouse model of Parkinson's disease. Parkinson's Dis 2017:1–7
28. Kordower JH, Olanow CW, Dodiya HB, Chu Y, Beach TG, Adler CH, Halliday GM, Bartus RT (2013) Disease duration and the integrity of the nigrostriatal system in Parkinson's disease. Brain 136:2419–2431